

Date of publication xxxx 00, 0000, date of current version xxxx 00, 0000.

Digital Object Identifier 10.1109/ACCESS.2017.Doi Number

Surpassing Cosine Similarity for Multidimensional Comparisons: Dimension Insensitive Euclidean Metric (DIEM)

Federico Tessari¹, Kunpeng Yao¹, Neville Hogan^{1,2}

¹Department of Mechanical Engineering, Massachusetts Institute of Technology, Cambridge, MA 02141 USA

² Department of Brain and Cognitive Sciences, Massachusetts Institute of Technology, Cambridge, MA 02141 USA

Corresponding author: Federico Tessari (e-mail: ftessari@mit.edu).

This work was supported by the Eric P. and Evelyn E. Newman Fund.

ABSTRACT Advancements in computational power and hardware efficiency have enabled the tackling of increasingly complex and high-dimensional problems. While artificial intelligence (AI) achieved remarkable results, the interpretability of high-dimensional solutions remains challenging. A critical issue is the comparison of multidimensional quantities, which is essential in techniques like Principal Component Analysis (PCA), or k-means clustering. Common metrics such as cosine similarity, Euclidean distance, and Manhattan distance are often used for such comparisons – for example in muscular synergies of the human motor control system. However, their applicability and interpretability diminish as dimensionality increases. This paper provides a comprehensive analysis of the effects of dimensionality on these metrics. Our results reveal significant limitations of cosine similarity, particularly its dependency on the dimensionality of the vectors, leading to biased and poorly interpretable outcomes. To address this, we introduce the Dimension Insensitive Euclidean Metric (DIEM) which demonstrates superior robustness and generalizability across dimensions. DIEM maintains consistent variability and eliminates the biases observed in traditional metrics, making it a reliable tool for high-dimensional comparisons. This novel metric has the potential to replace cosine similarity, providing a more accurate and insightful method to analyze multidimensional data in fields ranging from neuromotor control to machine and deep learning.

INDEX TERMS Cosine Similarity, Distance Measurement, Dimensionality Reduction, Euclidean Distance, Information Retrieval

I. INTRODUCTION

The continuous growth of computational capabilities combined with the improvement of hardware efficiency [1] granted the possibility to approach problems of growing complexity and dimensionality. Over a little more than two decades, Artificial intelligence (AI) agents were able to defeat humans in games considered – up to that point – dominated by humans: chess [2], Go [3], StarCraft II [4]. This capability to handle very complex and high-dimensional problems also led to promising results in different fields such as molecular biology [5] or robotics [6]. On one hand, the results of these computing techniques are undeniably impressive; on the other hand, their interpretability appears to decrease with their complexity and dimensionality.

Among the difficulties in the interpretation of these tools, a concern is the comparison of multidimensional quantities. For example, in dimensionality reduction techniques, such as Principal Component Analysis (PCA), Singular Value

Decomposition (SVD), or k-means clustering, the algorithms extract significant combinations of a selected set of input features. The number of input features can vary greatly, from tens – for example when considering the joint angles of the hand [7] – to hundreds such as when looking at high density electromyograms. A reasonable question that arises from this extraction process is: “How similar or different are these combinations of features from different data sources e.g., subjects, experiments, or iterations?”

Two practical examples might provide a better understanding. Consider, for instance, the task of identifying the individual user preferences for movies based on a series of input features such as the movies the user has watched, his/her evaluation of the movies, and the date when they were watched [8]. Alternatively, consider the task of identifying during a given motor task e.g., grasping an object, how a certain individual coordinates his/her different joints (shoulder, elbow, wrist, phalanges) to successfully complete

that motor action [9], [10]. Assuming the algorithm identifies specific individuals' preferences based on those given input features, how can we compare two different individuals' preferences? Answering this question is interesting because it can provide insight on the individuals' decision-making processes (movie example) or underlying control strategies (motor control example).

As long as the number of input features is limited to 2 or 3, humans are visually able to interpret them using a planar or spatial analogy. However, when feature spaces go beyond 3D, visualization and interpretation become more complex and less intuitive. As a consequence, researchers typically rely on mathematical measurements that provide an alternative understanding of the similarity (or difference) between n -dimensional quantities.

Among the most widely adopted methods for multidimensional comparisons, cosine similarity stands as one of the gold standards [11], [12], [13], [14], [15], [16]. The main reasons behind its use are likely related to its analogy with angular measurements and its bounded and well-defined range (between 0 and 1, or -1 and 1, depending on which formulation is used). Alternatives to cosine similarity have been proposed using, for example: (i) inner-product approximations [17], (ii) 'norms' or distance metrics, such as the Manhattan distance (1-norm) or the Euclidean distance (2-norm), (iii) or combinations of existing methods [18]. Interestingly, the interpretation of these comparison metrics is often limited to lower dimensional cases (2D or 3D), and it is typically extrapolated to higher dimensional cases without much justification.

In this work, we present a detailed analysis of the effects of dimensionality on three of the most common metrics for multidimensional comparison: cosine similarity, Euclidean distance and Manhattan distance. From the analysis of these metrics, some interesting limitations and properties emerge, leading to the conclusion that the use of cosine similarity might not be the most appropriate choice for multidimensional comparisons. An alternative to these three metrics, derived from the Euclidean distance, is proposed which shows better robustness and generalizability to increasing number of dimensions. The new metric – named DIEM (Dimension Insensitive Euclidean Metric) – is a candidate to surpass and replace the use of cosine similarity for high dimensional comparisons.

II. COSINE SIMILARITY AND EUCLIDEAN DISTANCE

Given two vectors $\mathbf{a} = [a_1 \dots a_n]$ and $\mathbf{b} = [b_1 \dots b_n]$, with $a_i, b_i \in \mathbb{R}$; the cosine similarity between these vectors is defined as:

$$\cos(\theta) = \frac{|\mathbf{a}^T \cdot \mathbf{b}|}{\|\mathbf{a}\| \cdot \|\mathbf{b}\|} \quad (1)$$

This value ranges between 0 and 1, with 0 meaning the two vectors are orthogonal, and 1 meaning the vectors are collinear. This measure is often used in the study of

kinematic and muscle synergies (identified via principal components) to estimate the degree of similarity between such principal components. This is done because each principal component can be considered a direction in the hyperspace that contains it.

A. Relation to Euclidean Distance

We can consider the \mathbf{a} and \mathbf{b} vectors as points in an n -dimensional space, and we can compute the Euclidean distance i.e., 2-norm, between them as:

$$d = \sqrt{\sum_{i=1}^n (a_i - b_i)^2} \quad (2)$$

This relation can be reworked to obtain:

$$\begin{aligned} d &= \sqrt{\sum_{i=1}^n (a_i - b_i)^2} = \sqrt{\sum_{i=1}^n (a_i^2 - 2a_i b_i + b_i^2)} \Rightarrow d^2 \\ &= \sum_{i=1}^n (a_i^2 - 2a_i b_i + b_i^2) \Rightarrow \\ d^2 &= \sum_{i=1}^n a_i^2 + \sum_{i=1}^n b_i^2 - 2 \sum_{i=1}^n a_i b_i \quad (3) \end{aligned}$$

We can then reformulate Eq. 1 in index notation:

$$\cos(\theta) = \frac{|\mathbf{a}^T \cdot \mathbf{b}|}{\|\mathbf{a}\| \cdot \|\mathbf{b}\|} = \frac{|\sum_{i=1}^n a_i b_i|}{\|\mathbf{a}\| \cdot \|\mathbf{b}\|} \quad (4)$$

Remembering that the Euclidean norm of a vector is equal to $\|\mathbf{x}\| = \sqrt{\sum_{i=1}^n x_i^2}$, and combining Equation 4 and Equation 3, we obtain:

$$\cos(\theta) = \frac{1}{\|\mathbf{a}\| \cdot \|\mathbf{b}\|} \cdot \left| \frac{\|\mathbf{a}\|^2 + \|\mathbf{b}\|^2 - d^2}{2} \right| \quad (5)$$

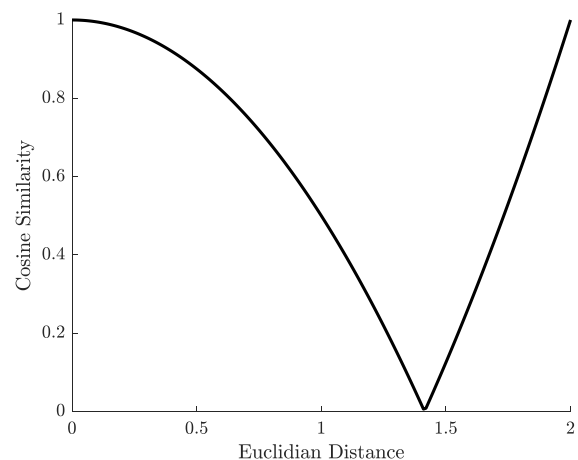


FIGURE 1. Graphical representation of the relation between cosine similarity and Euclidean distance for unit length vectors.

Equation (5) shows that the cosine similarity has a quadratic correlation with the Euclidean distance. Moreover, in the

case in which our vectors \mathbf{a}, \mathbf{b} present unit length, this relation simplifies to:

$$\cos(\theta) = \left| 1 - \frac{d^2}{2} \right| \quad (6)$$

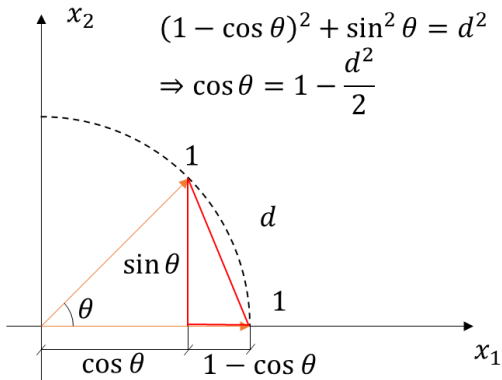


FIGURE 2. Geometrical relation between the angle spanned by two unit vectors and the Euclidean distance between their end points.

For unit-length vectors, the Euclidean distance can only range between $0 \leq d \leq 2$, since the vectors – independently of the dimension of space that they span – could at most be on a diameter of a hyper-sphere of radius 1. Figure 1 provides a graphical representation of Equation (6).

Equation 6 can also be derived using Pythagoras’ theorem on the red triangle highlighted in Figure 2.

An alternative definition of the cosine similarity excludes the absolute value of the scalar product in Equation 1. This alternative definition result in the cosine similarity spanning from -1 to 1. This includes also sign differences in the analyzed vectors. The relation with the Euclidean distance remains similar and it is treated for completeness in the Appendix.

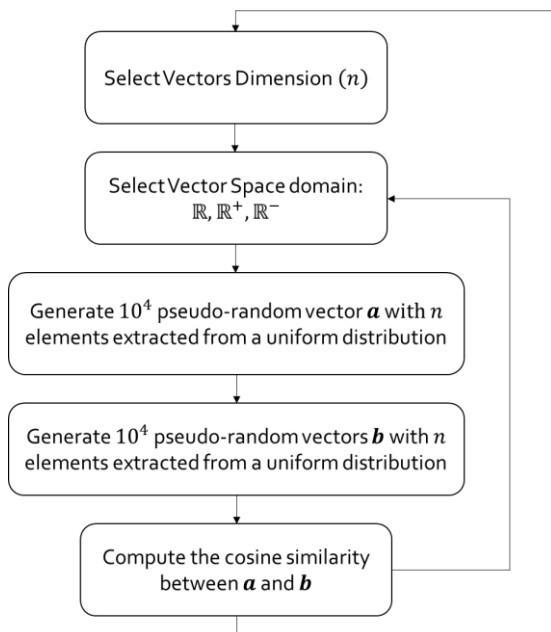


FIGURE 4. Algorithm used for the sensitivity analysis of the cosine similarity with respect to vectors’ dimension and domain.

III. EFFECT OF VECTORS’ DIMENSIONALITY

A second interesting aspect is the sensitivity of the cosine similarity metric to the dimension of the considered vectors (n) as well as to the space spanned by them: $\mathbb{R}^n, \mathbb{R}^{n+}, \mathbb{R}^{n-}$.

In order to test the sensitivity to these two aspects, a numerical simulation was run using the algorithm presented in Figure 3.

The idea was to iterate through growing dimensions while comparing two randomly generated vectors (\mathbf{a}, \mathbf{b}).

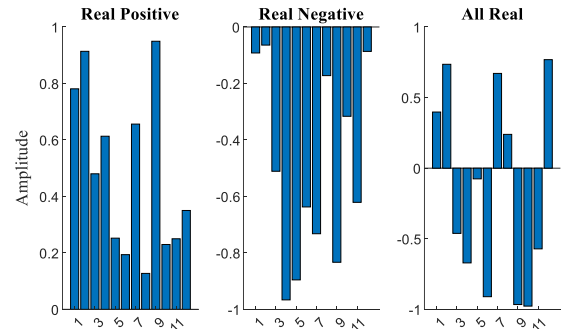


FIGURE 3. Three randomly generated vectors from the real positive, real negative and all real domains. Each element was extracted from a pseudo-uniform distribution with preset ranges.

The vectors were generated from a pseudo-uniform distribution in order to avoid bias on the mean value of each vector’s elements. The cosine similarity was computed for a range of dimensions going from 2 (planar case) to 102.

Vectors \mathbf{a}, \mathbf{b} were scaled such that, in the three different domains, their lengths assumed the following range of values: $\mathbb{R} \rightarrow -1 \leq a_i, b_i \leq 1 \forall i$, $\mathbb{R}^+ \rightarrow 0 \leq a_i, b_i \leq 1 \forall i$, $\mathbb{R}^- \rightarrow -1 \leq a_i, b_i \leq 0 \forall i$. Figure 4 shows three randomly generated vectors of dimension $n = 12$ for the three aforementioned ranges.

These ranges were arbitrarily chosen to resemble the activation level of some feature e.g., a surface electromyographic signal normalized to maximum voluntary activation. A sensitivity analysis of the vector scaling

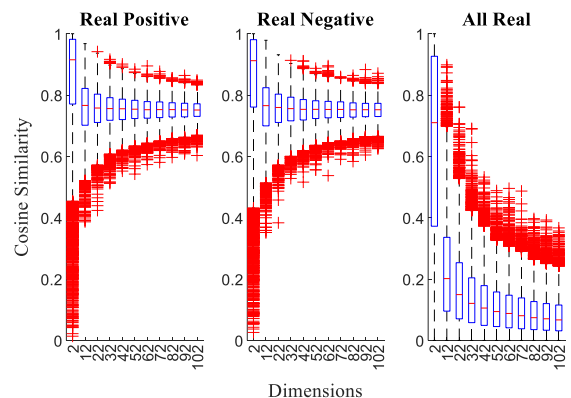


FIGURE 5. Cosine similarity boxplots for increasing dimension of the vectors \mathbf{a} and \mathbf{b} . The three panels show, respectively, the case in which vectors elements were only positive (left), only negative (center) or could assume all real values within the given range (right).

demonstrated that it produced no effect on cosine similarity. The resulting cosine similarities for each vector dimension and each vector domain are presented in Figure 5.

Interestingly, the growing dimensionality of these random vectors led to a convergence of the average cosine similarity. For the only-positive or only-negative vectors, cosine similarity rapidly converged to a value of about 0.75 ± 0.1 . For the vectors that could span both negative and positive values, the cosine similarity converged to a value approaching 0. In the Appendix, readers can find a

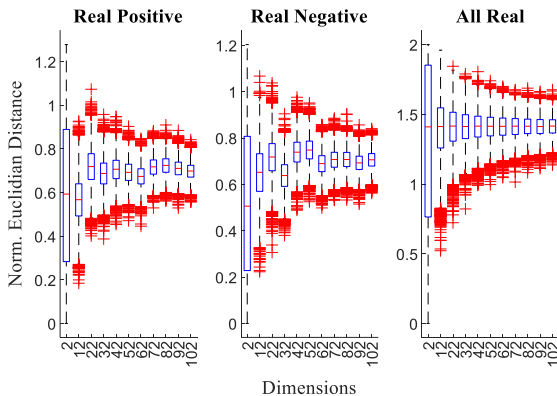


FIGURE 7. Normalized Euclidean distance for increasing dimension of the vectors a and b . The three panels show, respectively, the case in which vectors elements were only positive (left), only negative (center) or could assume all real values within the given range (right).

probabilistic theoretical proof of the convergence of cosine similarity in both the strictly positive, strictly negative and all real cases.

The numerical analysis proposed in Figure 3 has been replicated using, as comparison metric, the Euclidean distance between normalized vectors (Figure 6).

Also in this case, the normalized Euclidean distance converged toward a constant value with limited variability. Specifically, for the real positive and negative cases the metric converged to about 0.7 ± 0.1 , while for the all-real case it converged to 1.41 ± 0.2 . This value is close to $\sqrt{2}$, which is the expected distance between two unit vectors perfectly orthogonal to each other. In fact, for the all-real case of Figure 5, we observed the cosine similarity converging towards zero i.e., the vectors approached orthogonality.

A more troubling aspect – emerging from both the cosine similarity and normalized Euclidean distance (Figures 5 and 6) – was the fact that the scatter i.e., variability, of these metrics was a strong function of the number of dimensions (n). Specifically, the variability of these random comparisons tended to narrow with the increase of number of dimensions. Different distributions for sampling the vectors a, b , such as the Gaussian or uniform spherical distribution, were tested showing equivalent results to what is presented in Figures 5 and 6. Please refer to the Appendix for further details. If,

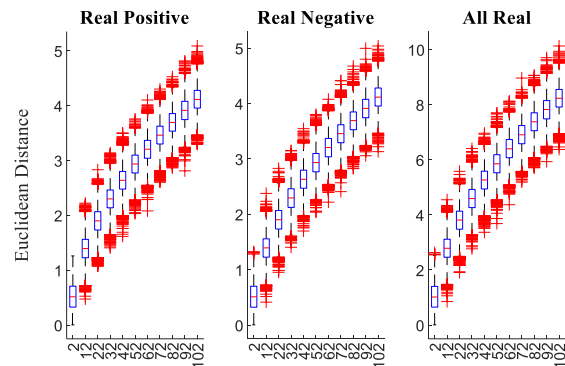


FIGURE 6. Euclidean distance for increasing dimension of the vectors a and b . The three panels show, respectively, the case in which vectors elements were only positive (left), only negative (center) or could assume all real values within the given range (right).

instead, we consider the non-normalized Euclidean distance, we observe the behavior presented in Figure 7.

The center of the Euclidean distance distribution tended to grow without bound, but the variability of each boxplot remained approximately constant. This is an improvement over the cosine similarity or normalized Euclidean distance case for two reasons: (i) the variability does not change with the dimension of the vectors a and b i.e., the variance (σ_{ed}^2) is only function of the range v_m, v_M but not of the number dimensions n , (ii) the metric does not converge towards a plateau.

IV. MATHEMATICAL PROPERTIES OF THE EUCLIDEAN DISTANCE

Some interesting properties can be analytically derived from the definition of Euclidean distance (Equation 2), assuming that each element of any two vectors a, b is bounded between a minimum v_m and maximum value v_M , with $v_M > v_m$. This boundedness is a reasonable assumption, since measurable physical quantities are typically bounded either by physical or measurement limitations.

Considering these assumptions, the minimum Euclidean distance between any two n -dimensional vectors a and b is always zero independent of dimension:

$$d_{min}(n) = 0 \quad \forall n \quad (7)$$

This is trivially demonstrated by assuming that:

$$\forall i = 1, \dots, n \rightarrow a_i = b_i \quad (8)$$

The maximum Euclidean distance can be computed considering that – for a given dimension n – each element of the vector a assumes its maximum value v_M , while each element of the other vector b assumes its minimum value v_m . At that point, the Euclidean distance of Equation 2 becomes:

$$\begin{aligned} d &= \sqrt{\sum_{i=1}^n (a_i - b_i)^2} \leq \sqrt{\sum_{i=1}^n (v_M - v_m)^2} \\ &= \sqrt{n(v_M - v_m)^2} \Rightarrow \\ d_{max}(n) &= \sqrt{n} \cdot (v_M - v_m) \quad (9) \end{aligned}$$

Moreover, assuming the elements of the two vectors (a, b) are sampled from two independent and identically distributed

(i.i.d.) random variables with uniform distributions: $a_i \sim U(v_m, v_M)$, $b_i \sim U(v_m, v_M)$; it is possible to analytically derive the upper bound of the expected Euclidean distance i.e., the main trend observed in Figure 7. Specifically, by applying Jensen's inequality¹ [19] and the "Law Of The Unconscious Statistician" (LOTUS) [20] we obtain:

$$\begin{aligned} E[d] &= E \left[\sqrt{\sum_{i=1}^n (a_i - b_i)^2} \right] \leq \sqrt{E \left[\sum_{i=1}^n (a_i - b_i)^2 \right]} \\ &= \sqrt{n \cdot E[(a - b)^2]} \\ &= \sqrt{n} \left(\int_{v_m}^{v_M} \int_{v_m}^{v_M} \frac{(a - b)^2}{(v_M - v_m)^2} da db \right)^{\frac{1}{2}} \quad (10) \end{aligned}$$

The integral in Equation 10 can easily be solved by direct integration. We leave readers the pleasure to do so. The final results can be expressed in the following form:

$$\begin{aligned} E[d] &\leq \sqrt{n} \sqrt{\frac{2}{3}(v_M^2 + v_M v_m + v_m^2) - \frac{1}{2}(v_M + v_m)^2} \\ &= \sqrt{\frac{n}{6}}(v_M - v_m) \quad (11) \end{aligned}$$

Equation 11 provides an analytical upper bound to the expected Euclidean distance between any two random vectors $\mathbf{a}, \mathbf{b} \sim U(v_m, v_M)$. Figure 8 provides a graphical representation of the Euclidean distance with also its maximum (Equation 9), minimum (Equation 7), and expected (Equation 11) value across dimensions.

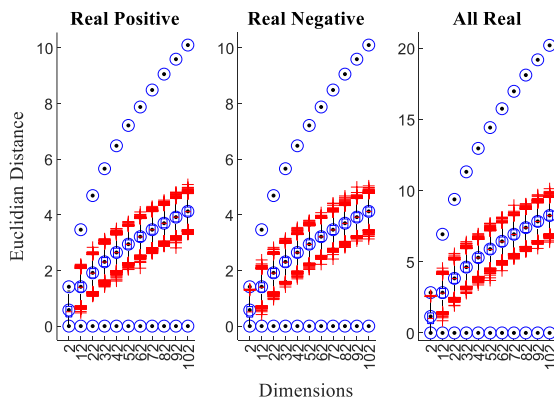


FIGURE 8. Euclidean distance for increasing dimensions of the vectors \mathbf{a} and \mathbf{b} . The three panels show, respectively, the case in which vector elements were only positive (left), only negative (center) or could assume all real values within the given range (right). The blue circles show the minimum, maximum and expected analytical Euclidean distance values.

Interestingly, the analytical expected value of the Euclidean distance (Eq. 11) is practically indistinguishable from the numerically simulated Euclidean distance median value, for any dimension $n > 2$. Moreover, it is also interesting to observe that the expected value is smaller than the arithmetic

mean between the maximum and minimum Euclidean distance:

$$\begin{aligned} \frac{d_{\min}(n) + d_{\max}(n)}{2} &= \frac{\sqrt{n}}{2}(v_M - v_m) \Rightarrow \\ \frac{\sqrt{n}}{2}(v_M - v_m) &> \sqrt{\frac{n}{6}}(v_M - v_m) \quad (12) \end{aligned}$$

Another interesting aspect to observe is the evolution of the Euclidean distance distribution for growing dimensions. The Real Positive case was considered, but equivalent results were obtained for Real Negative and All Real cases.

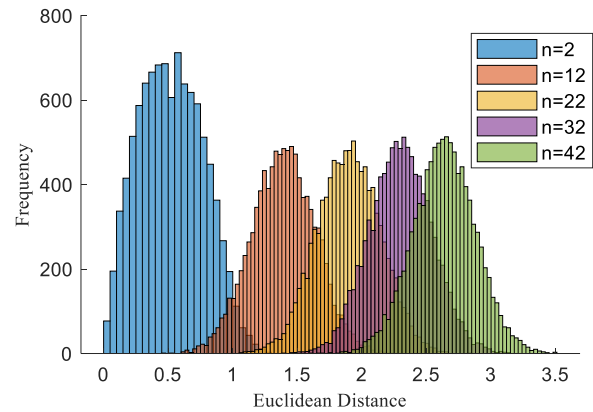


FIGURE 9. Histograms of the non-normalized Euclidean distance for growing dimensions 'n'.

For each of the simulated dimensions (n), a Kolmogorov-Smirnov test was performed to check whether the observed simulated distribution was significantly different from a normal distribution with mean and standard deviation equal to those of the simulated data $N(\text{mean}(d), \text{std}(d))$. Interestingly, the test showed a significant difference only for $n = 2$ ($p < 0.05$); while, for all the other tested dimensions the distribution of Euclidean distances was not significantly different from a normal distribution. A finer simulation on a subset of dimensions ($2 \leq n \leq 12$) revealed a smooth transition between non-normal and normal distribution around $n \cong 7$. Please refer to the Appendix for a detailed presentation of the transition between non-normal and normal distributions.

A confirmation of these results can be found in the work of Thirey and Hickam [21] in which they analytically derived the distribution of Euclidean distances between randomly distributed Gaussian vectors and observed a normalization of the distribution with increasing number of dimensions n . Despite this trend to normality of the distribution of Euclidean distances, it is important to emphasize that the distribution tails are not symmetric. This is clearly observable from Figure 8 and it finds demonstration in Equation 12, since the expected value $E[d]$ is smaller than the mean between the maximum and minimum Euclidean distance. This asymmetry suggests that the distribution of Euclidean distance is not properly normal though it is effectively indistinguishable from normal.

¹ Jensen's Inequality assumes concavity, and the square root function is indeed concave. This accounts for the 'less-than-or-equal' in Equation 10.

V. A DIMENSIONAL-INSENSITIVE METRIC FOR MULTIDIMENSIONAL COMPARISON

At this point, we can obtain a dimension-insensitive metric by subtracting from each Euclidean distance distribution its expected value ($E[d(n)]$) i.e., the main trend, normalize it by the variance (σ_{ed}^2) of the Euclidean distance ($\sqrt{\sum_{i=1}^n (a_i - b_i)^2}$) and scale it to the range of the analyzed quantities ($v_M - v_m$). The resulting metric has been named 'Dimension Inensitive Euclidean Metric' (DIEM):

$$DIEM = \frac{v_M - v_m}{\sigma_{ed}^2} \left(\sqrt{\sum_{i=1}^n (a_i - b_i)^2} - E[d(n)] \right) \quad (13)$$

The resulting distributions for the DIEM are presented in Figure 10.

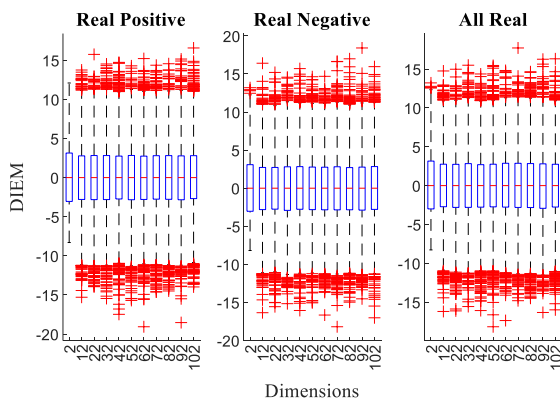


FIGURE 10. Dimension Inensitive Euclidean Metric (DIEM) for increasing dimension of the vectors a and b . The three panels show, respectively, the case in which vector elements were only positive (left), only negative (center) or could assume all real values within the given range (right).

Figure 10 shows that increasing the number of dimensions does not affect either the converged value nor the variance of the measurements, thus providing a more reliable comparison metric for high-dimensional vectors. Moreover, the histograms of Dimension Inensitive Euclidean Metric show how the distributions are practically identical for $n \geq 7$ (Figure 11). This facilitates precise statistical testing.

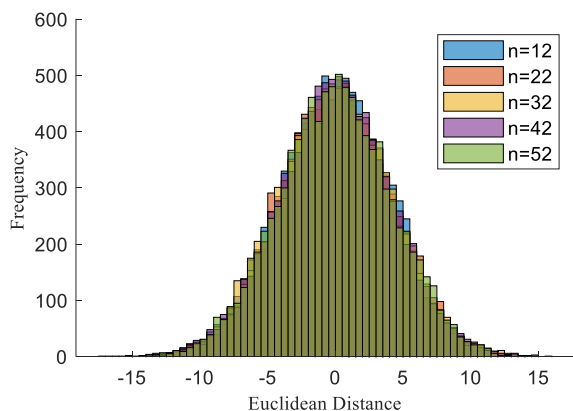


FIGURE 11. Histograms of the detrended Euclidean distance for growing dimensions 'n'.

A more intuitive understanding of similarity and dissimilarity using DIEM is provided in Figure 12. In general, vectors may have different magnitudes and orientations. Lower values of DIEM represent similar vectors, while higher values of the metric represent dissimilar vectors. Since the DIEM is detrended, its expected value $E[DIEM]$ is 0. The shaded red areas respectively show one, two and three standard deviations (σ). Three dotted lines are added to present, respectively, the maximum Dimension Inensitive Euclidean Metric ($DIEM_{max}$) – which represents antiparallel vectors with maximum magnitude, the average Dimension Inensitive Euclidean Metric between orthogonal vectors ($E[DIEM_{orth}]$) and the minimum Dimension Inensitive Euclidean Metric ($DIEM_{min}$) – which represents identical vectors.

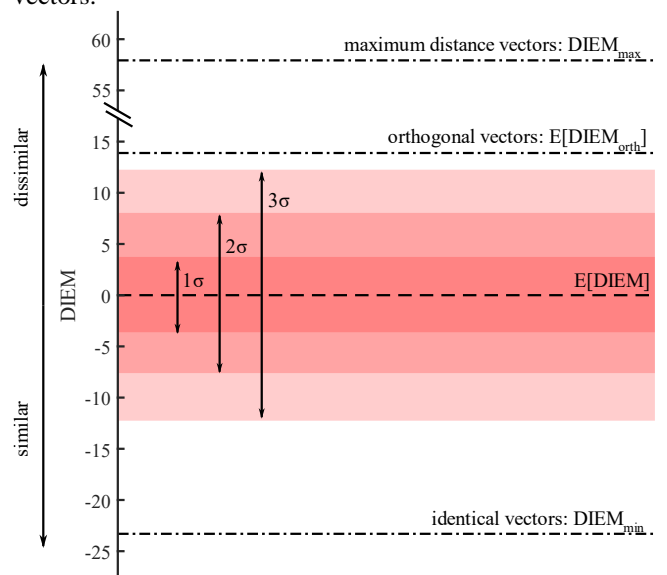


FIGURE 12. Explanatory scheme of the Dimension Inensitive Euclidean Metric (DIEM). This image was generated considering $n = 12, v_M = 1, v_m = 0, \sigma_{ed}^2 = 0.06$. The dashed black line represents the expected DIEM. The red colored bands represent respectively one ($\sigma = 4.09$), two and three standard deviations of the DIEM distribution. The top dotted black line is the maximum $DIEM_{max} = 58.09$, representing two opposing vectors with maximum magnitude. The second from top dotted black line is the median value of the DIEM for orthogonal vectors $E[DIEM_{orth}] = 13.96$. The bottom dotted black line is the minimum $DIEM_{min} = -23.42$, representing two identical vectors.

The mean Dimension Inensitive Euclidean Metric between orthogonal vectors ($E[DIEM_{orth}]$) was computed by generating a series of orthogonal vectors and numerically computing their expected value. From the considered case in Figure 12 ($n = 12, v_M = 1, v_m = 0, \sigma = 4.09$), the probability of two random vectors to be orthogonal was more than three standard deviations from the mean.

The minimum DIEM is easily obtained combining Equation (7) with Equation (13):

$$DIEM_{min} = - \frac{v_M - v_m}{\sigma_{ed}^2} E[d(n)] \quad (14)$$

while maximum DIEM is obtained considering Equation (9) in combination with Equation (13):

$$DIEM_{max} = \frac{v_M - v_m}{\sigma_{ed}^2} (\sqrt{n} \cdot (v_M - v_m) - E[d(n)]) \quad (15)$$

It is worth emphasizing that, while the expected value of the Dimension Insensitive Euclidean Metric ($E[DIEM]$) as well as its variance (and standard deviation) remain constant independent of the number of dimensions, the value of the maximum and minimum Dimension Insensitive Euclidean Metric ($DIEM_{max}, DIEM_{min}$) as well as the expected distance between orthogonal vectors ($E[DIEM_{orth}]$) are functions of $E[d(n)]$ and, thus, of the number of dimensions. Both quantities are, however, numerically computable either by numerical simulation ($E[DIEM_{orth}]$) or by direct derivation ($DIEM_{max}, DIEM_{min}$).

An interesting question is whether the mathematical properties of the Euclidean distance are unique to the 2-norm or generalize to different norms. In this context, another common metric for comparison of multidimensional vectors is the Manhattan distance or 1-norm. Considering two vectors \mathbf{a}, \mathbf{b} , each composed by n elements; the Manhattan distance is defined as:

$$d_M = \sum_{i=1}^n |a_i - b_i| \quad (15)$$

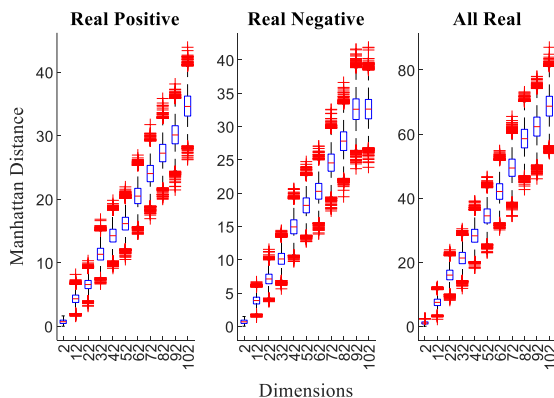


FIGURE 13. Manhattan distance for increasing dimension of the vectors \mathbf{a} and \mathbf{b} . The three panels show, respectively, the case in which vectors elements were only positive (left), only negative (center) or could assume all real values within the given range (right).

Applying the same algorithm presented in Figure 3, Figure 13 presents the Manhattan distance evolution with increasing dimensions (n). The Manhattan distance grows linearly with respect to the number of dimensions, and this can be demonstrated by calculating the maximum Manhattan distance value between two random vectors and realizing that it grows proportionally to n :

$$d_{M_{max}}(n) = n|v_{max} - v_{min}| \quad (16)$$

More importantly, the variance of the Manhattan distance does not remain constant with the increase in dimensions as it does for the Euclidean distance. It actually grows with dimensions. This is a limitation of its applicability for a dimension-insensitive metric compared to the Euclidean metric presented in this work. Higher order norms e.g., 3-

norm, 4-norm, and so on, could be attempted, but that investigation is not treated here.

The code to compute the DIEM is available at the following GitHub repository: <https://github.com/ftessari23/DIEM>

VI. DISCUSSION

In the study of multidimensional quantities (e.g., principal components extracted through PCA), cosine similarity is used – independently of the dimension – as a metric to assess similarity between such quantities. Our results show that such a metric is strongly influenced by the dimension of the investigated vector. For example, if we look in Figure 5 at dimension $n = 2$ (planar case), we observe – in all three cases – that the cosine angle between two random vectors \mathbf{a} and \mathbf{b} led to a broad almost uniform distribution of cosine similarity between 0 and 1, as we might expect. However, as soon as we moved away from the planar case ($n = 2$), the distribution of cosine similarity narrowed and converged, thus limiting the interpretability of this metric. Purely random vectors yielded an apparent similarity of about 0.75 for strictly positive (or negative) vectors, and 0 for all real vectors. That implies an included angle of about 41 degrees in the former case or 90 degrees in the latter. This means that randomly generated vectors in high dimensions will result in a constant orientation with respect to each other. This is a completely misleading way to compare quantities, as it risks leading a naïve investigator to consider two vectors to be very different (or very similar) based on pure chance.

A practical example can be derived from the study of muscle synergies. Let's imagine we extract muscle synergies using non-negative matrix factorization [22] from two different subjects performing the same task. We later want to compare the synergy composition that accounts for most of the variation between subjects. Such a synergy composition would typically look similar to what was presented in the left panel of Figure 4 i.e., an n -dimensional vector with n equal to the number of sampled muscles. The vector elements can assume only positive values, since post-processed muscular activity sampled through electromyography is typically rectified.

Now if n is greater than 2, as in many cases, our analysis in Figure 5 shows that any random vector extracted from the same distribution will tend to converge toward a similarity of 0.75 with a limited overall range. Therefore, if from our 2-synergy comparison we observe a similar value (say 0.75), we won't be able to determine whether such synergies are effectively similar to each other, or simply the result of a random chance. Similar considerations apply to synergies extracted from kinematic features, which are able to span the whole real range, thus following a behavior similar to the rightmost panel of Figure 5. This emphasizes the importance of considering the dimensionality of the considered vectors to correctly assess if the two vectors are effectively similar (collinear) or dissimilar (orthogonal).

Similar results are obtained when analyzing the normalized Euclidean distance, in agreement with Equation 6. However, if instead we consider the non-normalized

Euclidean distance, we achieve two interesting results (refer to Figure 7): (i) the metric is unbounded; the center of its distribution increases with the square root of the number of dimensions, (ii) its variability appears to remain constant. By detrending the Euclidean distance boxplots (Figure 10) – in our case using the expected value – we obtain a metric to measure the similarity or dissimilarity between hyper-dimensional vectors that is **insensitive** of the number of considered dimensions (n). This feature appears to be a particular property of the Euclidean distance. In fact, when using a different norm (Manhattan distance), the resulting behavior does not guarantee a dimension-insensitive variance (Figure 12). Moreover, for $n \geq 7$, the resulting distribution of detrended Euclidean distances is statistically indistinguishable from a normal distribution (Figure 11). This opens access to a very broad set of rigorous test methods for statistical comparisons e.g., t-tests or ANOVA. The analysis and comparison of multi-dimensional quantities – such as synergies in the human neuromotor control literature or principal components and clusters in deep learning methods – has represented a thorny and often ‘neglected’ problem. Most studies rely on comparison metrics e.g., the cosine similarity, without a complete understanding of their dependency on the number of dimensions of the considered features. Our study reveals that this dimensional dependency can significantly bias the interpretation of these metrics, leading to potentially erroneous conclusions. In response to this challenge, we introduce the Dimension Insensitive Euclidean Metric (DIEM), which effectively mitigates the dimensional dependency issue, providing a more accurate and interpretable measure for multi-dimensional comparisons. DIEM’s ability to maintain consistent variability across dimensions opens new avenues for robust statistical analysis and hypothesis testing, facilitating deeper insights into complex data structures. By adopting DIEM, researchers can enhance the reliability of their multi-dimensional analyses, paving the way for more precise and meaningful interpretations in fields ranging from neuromotor control to deep learning. Future research should continue to explore and refine this metric, ensuring its broad applicability and further validating its advantages over traditional methods.

APPENDIX

A. SIGNED COSINE SIMILARITY

The cosine similarity can also be presented as:

$$\cos(\theta) = \frac{\mathbf{a}^T \cdot \mathbf{b}}{|\mathbf{a}| \cdot |\mathbf{b}|} \quad (17)$$

Where the vectors \mathbf{a} and \mathbf{b} are defined as: $\mathbf{a} = [a_1 \dots a_n]$ and $\mathbf{b} = [b_1 \dots b_n]$, with $a_i, b_i \in \mathbb{R}$.

In this case, the cosine similarity spans from -1 (opposing vectors) to 1 (aligned vectors), with 0 representing orthogonal vectors’.

The mathematical relation between this alternative definition of the cosine similarity and the Euclidean distance remains equivalent. Equations 5 and 6 become:

$$\cos(\theta) = \frac{1}{|\mathbf{a}| \cdot |\mathbf{b}|} \cdot \frac{|\mathbf{a}|^2 + |\mathbf{b}|^2 - d^2}{2} \quad (18)$$

$$\cos(\theta) = 1 - \frac{d^2}{2} \quad (19)$$

The signed cosine similarity still presents a quadratic relation with the Euclidean distance. The considerations on the convergence of the cosine similarity remain valid.

B. EFFECT OF VECTORS’ DISTRIBUTION

The effect of dimensionality on randomly generated vectors (\mathbf{a}, \mathbf{b}) was tested on elements drawn from three different distributions: (i) uniform (Figure 4), (ii) Gaussian (Figure S1), (iii) uniformly distributed on a unit sphere (Figure S2) [23], [24]. The same algorithm proposed in Figure 3 was adopted.

In the Gaussian distribution case, the elements of the vectors (\mathbf{a}, \mathbf{b}) were sampled from Gaussian distributions with mean and standard deviation respectively equal to: real positive $\mu = 0.5, \sigma = 0.3$, real negative $\mu = -0.5, \sigma = 0.3$, all real $\mu = 0, \sigma = 0.6$.

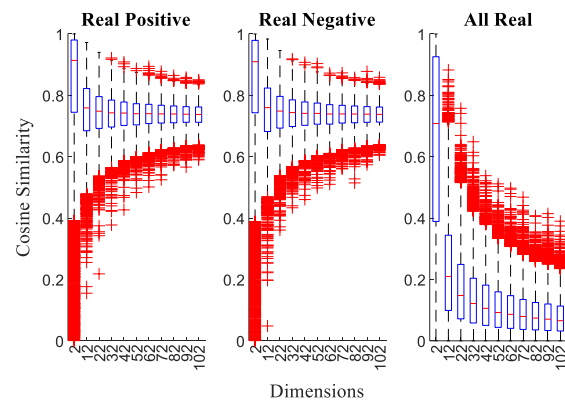


FIGURE S1. Cosine similarity boxplots for increasing dimension of the vectors \mathbf{a} and \mathbf{b} . The three panels show, respectively, the case in which vector elements were only positive (left), only negative (center) or could assume all real values within the given range (right). The elements of the vectors were sampled from a Gaussian distribution.

In the case of a uniform unit sphere distribution, the elements of the vectors (\mathbf{a}, \mathbf{b}) were sampled from a uniform distribution following the approach presented in the main manuscript (Section “Effects of Vectors’ Dimensionality”) and then projected to a unit n-sphere following the algorithm presented in the works by Marsaglia and Muller [23], [24].

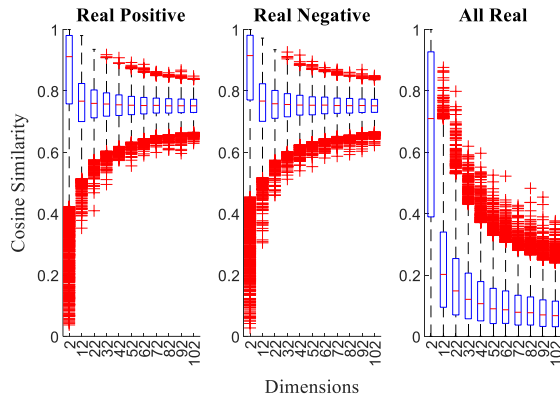


FIGURE S2. Cosine similarity boxplots for increasing dimension of the vectors \mathbf{a} and \mathbf{b} . The three panels show, respectively, the case in which vectors elements were only positive (left), only negative (center) or could assume all real values within the given range (right). The elements of the vectors were sampled from a uniform unit n -sphere distribution.

Figure S1 and S2 align with the results presented in Figure 4, confirming that the cosine similarity metric shows a converging trend with decreasing variance for every tested distribution. The reason for this behavior can be attributed to the normalization of the vectors (\mathbf{a}, \mathbf{b}) in the mathematical formulation of the cosine similarity (Equation 1). This normalization causes the considered distributions to ‘collapse’ onto a unit n -dimensional sphere.

In the authors’ opinion, a uniform distribution is the most representative of a real scenario especially when the vectors represent physical quantities. For example, if the elements of the vectors \mathbf{a}, \mathbf{b} are physical quantities – such as force or position – acquired through sensors, they will arguably have the same probability to be sampled between the minimum ‘ v_m ’ and maximum ‘ v_M ’ of the sensor sampling range, thus justifying the uniform distribution. However, for completeness we explored distributions that might occur in different data processing conditions.

Figure S3 provides an intuitive bi-dimensional understanding of the difference between vectors (or points) sampled from the uniform, Gaussian and uniformly distributed unit sphere distributions. Despite these different distributions, Figures S1, S2 and Figure 4 show that the main trends used to define DIEM were observed in all cases.

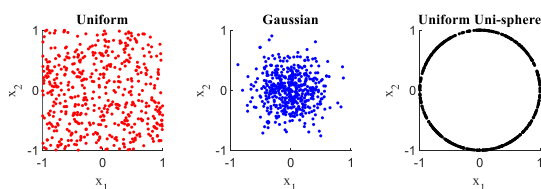


FIGURE S3. Two dimensional points sampled with from three different distributions. The left plot (red dots) shows points sampled from a uniform distribution $U(-1, 1)$. The central plot (blue dots) shows points sampled from a Gaussian distribution with mean 0 and standard deviation 0.3. The right plot (black dots) shows points sampled from a uniform distribution on the unit sphere ($r = 1$).

C. TRANSITION FROM NON-NORMAL TO NORMAL DISTRIBUTION

We observed that the distribution of Euclidean distances between randomly generated vectors tended to become normal with the increase of the vectors’ dimension. Here we present the result of a finer simulation that shows the transition between non-normal and normal distribution. All the three cases (Real Positive, Real Negative and All Real) were considered and yielded equivalent results.

The simulation was performed considering vectors’ dimensions spanning from $n = 2$ to $n = 12$. Kolmogorov-Smirnov tests were performed to check whether the observed simulated distribution was significantly different from a normal distribution with mean and standard deviation equal to those of the simulated data $N(\text{mean}(d), \text{std}(d))$. A p-value $p < 0.05$ was consistently observed for distributions with $n < 5$, while it presented consistently $p > 0.05$ for $n > 7$. Figure S4 presents the trend of Euclidean distance distribution for the Real Positive case in the range $2 \leq n \leq 12$. The results confirm a smooth transition between a non-normal to a normal distribution for $n > 7$.

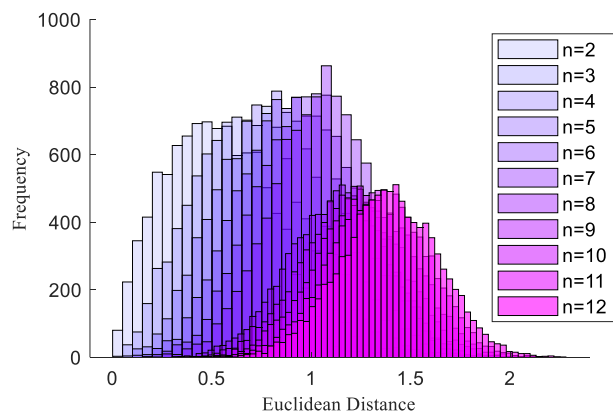


FIGURE S4. Histograms of the non-normalized Euclidean distance for growing dimensions n in the range $2 \leq n \leq 12$.

D. PROOF OF CONVERGENCE OF COSINE SIMILARITY

All Real Case

Consider two vectors $\mathbf{a}, \mathbf{b} \in \mathbb{R}^n$ and assume these vectors are independently sampled on the uniform unit-sphere such that $\|\mathbf{a}\| = \|\mathbf{b}\| = 1$.

The cosine similarity i.e., the angle between these vectors, will follow Equation (1), unsigned version, or Equation (17) signed version. For simplicity, but without loss of accuracy, we consider the form in Equation (17):

$$\cos(\theta) = \frac{\mathbf{a}^T \cdot \mathbf{b}}{\|\mathbf{a}\| \cdot \|\mathbf{b}\|} = \mathbf{a}^T \cdot \mathbf{b} = \sum_{i=1}^n a_i b_i \quad (20)$$

Since \mathbf{a} and \mathbf{b} are i.i.d. uniformly distributed on the unit sphere centered around 0, each of their entries a_i and b_i has zero mean:

$$E[a_i] = E[b_i] = 0 \quad (21)$$

This is due to the symmetry of the unit sphere. As a consequence, the expectation of the inner product i.e., the cosine of their angle, is equal to:

$$E[\mathbf{a}^T \cdot \mathbf{b}] = E\left[\sum_{i=1}^n a_i b_i\right] = \sum_{i=1}^n E[a_i]E[b_i] = 0 \quad (22)$$

This is already sufficient to show that the expected value of the cosine similarity between uniformly distributed points on a unit-sphere is 0, and thus their resulting angle is 90 degrees.

To show the convergence for higher dimensions, we can compute the variance of the cosine similarity:

$$\begin{aligned} \text{Var}(\mathbf{a}^T \cdot \mathbf{b}) &= E[(\mathbf{a}^T \cdot \mathbf{b})^2] - (E[\mathbf{a}^T \cdot \mathbf{b}])^2 = \\ &= E[(\mathbf{a}^T \cdot \mathbf{b})^2] \quad (23) \end{aligned}$$

Expanding the square of the inner product we obtain:

$$\begin{aligned} (\mathbf{a}^T \cdot \mathbf{b})^2 &= \left(\sum_{i=1}^n a_i b_i\right)^2 = \\ &= \sum_{i=1}^n a_i^2 b_i^2 + 2 \sum_{i < j} a_i b_i a_j b_j \quad (24) \end{aligned}$$

Taking expectations:

$$\begin{aligned} E[(\mathbf{a}^T \cdot \mathbf{b})^2] &= E\left[\left(\sum_{i=1}^n a_i b_i\right)^2\right] = \\ &= E\left[\sum_{i=1}^n a_i^2 b_i^2 + 2 \sum_{i < j} a_i b_i a_j b_j\right] = \\ &= E\left[\sum_{i=1}^n a_i^2 b_i^2\right] + 2E\left[\sum_{i < j} a_i b_i a_j b_j\right] \quad (25) \end{aligned}$$

Since a_i and b_i are i.i.d., we have:

$$E\left[\sum_{i < j} a_i b_i a_j b_j\right] = 0 \quad (26)$$

Hence:

$$E[(\mathbf{a}^T \cdot \mathbf{b})^2] = E\left[\sum_{i=1}^n a_i^2 b_i^2\right] = \sum_{i=1}^n E[a_i^2]E[b_i^2] \quad (27)$$

However, since \mathbf{a} and \mathbf{b} are on the unit-sphere, their norm is equal to 1:

$$\|\mathbf{a}\| = \|\mathbf{b}\| = \sum_{i=1}^n a_i^2 = \sum_{i=1}^n b_i^2 = 1 \quad (28)$$

Therefore:

$$\begin{aligned} E\left[\sum_{i=1}^n a_i^2\right] &= nE[a_i^2] = 1 \\ \Rightarrow E[a_i^2] &= \frac{1}{n} = E[b_i^2] \quad (29) \end{aligned}$$

Substituting Equation (29) in Equation (25), we obtain:

$$E[(\mathbf{a}^T \cdot \mathbf{b})^2] = n \left(\frac{1}{n} \cdot \frac{1}{n}\right) = \frac{1}{n} \quad (30)$$

We finally obtain that the variance of the cosine similarity between \mathbf{a} and \mathbf{b} is equal to:

$$\text{Var}(\mathbf{a}^T \cdot \mathbf{b}) = \frac{1}{n} \quad (31)$$

According to Equation (31) the variance of the cosine similarity for uniformly sampled vectors on the unit-sphere decreases with the increase of dimensions. Moreover, from the Centra Limit Theorem, we can write that the cosine similarity assumes a normal distribution with mean 0 and variance $1/n$:

$$\cos(\theta) = \mathbf{a}^T \cdot \mathbf{b} \sim N\left(0, \frac{1}{n}\right) \quad (32)$$

For completeness, we demonstrate the convergence of this distribution for $n \rightarrow \infty$. To do this, we can consider Chebyshev's inequality for a random variable X with mean μ and variance σ^2 :

$$\Pr(|X - \mu| \geq k\sigma) \leq \frac{1}{k^2}, \forall k \in \mathbb{R}^+ \quad (33)$$

Applying Equation (33) to our cosine similarity distribution we obtain:

$$\begin{aligned} \Pr(|\cos(\theta)| \geq \alpha) &= \Pr(|\mathbf{a}^T \cdot \mathbf{b}| \geq \alpha) \leq \frac{\sigma^2}{\alpha^2} \text{ with } \alpha = k\sigma \\ \Rightarrow \Pr(|\cos(\theta)| \geq \alpha) &\leq \frac{\text{Var}(\mathbf{a}^T \cdot \mathbf{b})}{\alpha^2} = \frac{1}{n\alpha^2} \quad (34) \end{aligned}$$

The limit for $n \rightarrow \infty$ of $\frac{1}{n\alpha^2}$ is equal to 0, while $\Pr(\cdot) \geq 0$. As a consequence:

$$\begin{aligned} \lim_{n \rightarrow \infty} \Pr(|\cos(\theta)| \geq \alpha) &= 0, \forall \alpha \in \mathbb{R}^+ \\ \Rightarrow \lim_{n \rightarrow \infty} |\cos(\theta)| &= 0 \quad (35) \end{aligned}$$

Therefore, as $n \rightarrow \infty$ the vectors \mathbf{a} and \mathbf{b} will be orthogonal with shrinking variance. This demonstrates the convergence observed in Figure 5 for the all-real case.

Real Positive Case

Unlike the all-real case, we consider now the elements of the vectors \mathbf{a} and \mathbf{b} sampled for i.i.d. of the type $a_i, b_i \sim U(0,1)$. In this case, the vectors are no longer unit vectors, and the cosine similarity remains equal to Equation (17): $\cos(\theta) = \frac{\mathbf{a}^T \cdot \mathbf{b}}{\|\mathbf{a}\| \cdot \|\mathbf{b}\|}$.

Recalling the generic uniform distribution $X \sim U(a, b)$, we know that:

$$E[X] = \frac{1}{2}(a + b), \text{Var}(X) = \frac{1}{12}(b - a)^2 \quad (36)$$

Therefore, applying Equation (36) to our case, we obtain:

$$E[a_i] = E[b_i] = \frac{1}{2}, \text{Var}(a_i) = \text{Var}(b_i) = \frac{1}{12} \quad (37)$$

We can now compute the expectation as follows:

$$\begin{aligned} E[a_i b_i] &= E[a_i]E[b_i] = \frac{1}{4} \\ E[a_i^2] &= E[b_i^2] = \int_0^1 a^2 da = \frac{1}{3} \\ E[(a_i b_i)^2] &= E[a_i^2]E[b_i^2] = \frac{1}{9} \\ E[a_i^3] &= E[b_i^3] = \int_0^1 a^3 da = \frac{1}{4} \\ E[a_i^4] &= E[b_i^4] = \int_0^1 a^4 da = \frac{1}{5} \end{aligned} \quad (38)$$

The variances will, then, result:

$$\begin{aligned} \text{Var}(a_i b_i) &= E[(a_i b_i)^2] - (E[a_i b_i])^2 = \\ &= \frac{1}{9} - \left(\frac{1}{4}\right)^2 = \frac{7}{144} \\ \text{Var}(a_i^2) &= \text{Var}(b_i^2) = E[(a_i^2)^2] - (E[a_i^2])^2 = \\ &= \frac{1}{5} - \frac{1}{9} = \frac{4}{45} \end{aligned} \quad (39)$$

To simplify the cosine similarity expression, we define the following quantities:

$$A_n = \sum_{i=1}^n a_i b_i, B_n = \sum_{i=1}^n a_i^2, C_n = \sum_{i=1}^n b_i^2 \quad (40)$$

Then, the cosine similarity equation becomes:

$$\cos(\theta) = \frac{\mathbf{a}^T \cdot \mathbf{b}}{\|\mathbf{a}\| \cdot \|\mathbf{b}\|} = \frac{A_n}{\sqrt{B_n C_n}} \quad (41)$$

We can now decompose each term in Equation (41) in its expected value plus a fluctuation term to analyze the behavior for $n \rightarrow \infty$:

$$\begin{aligned} A_n &= nE[a_i b_i] + \delta_{A_n} = \frac{n}{4} + \delta_{A_n}, \\ B_n &= nE[a_i^2] + \delta_{B_n} = \frac{n}{3} + \delta_{B_n}, \\ C_n &= nE[b_i^2] + \delta_{C_n} = \frac{n}{3} + \delta_{C_n} \end{aligned} \quad (42)$$

The associated fluctuation terms are equal to:

$$\begin{aligned} \delta_{A_n} &= \sum_{i=1}^n (a_i b_i - E[a_i b_i]), \\ \delta_{B_n} &= \sum_{i=1}^n (a_i^2 - E[a_i^2]), \\ \delta_{C_n} &= \sum_{i=1}^n (b_i^2 - E[b_i^2]) \end{aligned} \quad (43)$$

The fluctuations δ_{A_n} , δ_{B_n} , and δ_{C_n} are sums of i.i.d. random variables with zero mean. Therefore, according to the Central Limit Theorem, the sum of a large number of i.i.d. random variables with finite mean and

variance will be approximately normally distributed, regardless of the original distribution of the variables. Mathematically, for i.i.d. random variable z_i with mean μ and standard deviation σ , its sum $S = \sum_{i=1}^n z_i$ satisfies:

$$\lim_{n \rightarrow \infty} \frac{S - n\mu}{\sqrt{n}\sigma} \sim N(0,1) \quad (44)$$

Using the sum of i.i.d. random variable $\text{Var}(X + Y) = \text{Var}(X) + \text{Var}(Y)$, we can calculate the standard deviations of the terms A_n , B_n , and C_n as follows:

$$\begin{aligned} \sigma_A &= \sqrt{n \text{Var}(a_i b_i)} = \frac{\sqrt{7n}}{12}, \\ \sigma_B &= \sigma_C = \sqrt{n \text{Var}(a_i^2)} = 2\sqrt{\frac{n}{45}} \end{aligned} \quad (45)$$

Since we only care about the order of the fluctuations, we can consider that:

$$\delta_{A_n} = \delta_{B_n} = \delta_{C_n} = O(\sqrt{n}) \quad (46)$$

Hence:

$$\frac{\delta_{A_n}}{n} = \frac{\delta_{B_n}}{n} = \frac{\delta_{C_n}}{n} = O\left(\frac{1}{\sqrt{n}}\right) \quad (47)$$

We can now expand the cosine similarity presented in Equation (41) using Equation (42):

$$\cos(\theta) = \frac{A_n}{\sqrt{B_n C_n}} = \frac{\frac{n}{4} + \delta_{A_n}}{\sqrt{\left(\frac{n}{3} + \delta_{B_n}\right)\left(\frac{n}{3} + \delta_{C_n}\right)}} \quad (48)$$

The denominator of Equation (48) can be further simplified by re-expressing it in a different form and using the binomial approximation expansion truncated at the first-order terms ($\sqrt{(1+b)(1+c)} \approx 1 + \frac{b+c}{2}$):

$$\begin{aligned} \sqrt{B_n C_n} &= \frac{n}{3} \sqrt{\left(1 + \frac{3\delta_{B_n}}{n}\right)\left(1 + \frac{3\delta_{C_n}}{n}\right)} \approx \\ &\approx \frac{n}{3} \left(1 + \frac{3}{2n}(\delta_{B_n} + \delta_{C_n})\right) = \frac{n}{3} + \frac{1}{2}(\delta_{B_n} + \delta_{C_n}) \end{aligned} \quad (49)$$

Plugging Equation (49) in Equation (48) we obtain:

$$\begin{aligned} \cos(\theta) &= \frac{A_n}{\sqrt{B_n C_n}} \approx \frac{\frac{n}{4} + \delta_{A_n}}{\frac{n}{3} + \frac{1}{2}(\delta_{B_n} + \delta_{C_n})} = \\ &= \frac{\frac{1}{4} + \frac{\delta_{A_n}}{n}}{\frac{1}{3} + \frac{1}{2}\left(\frac{\delta_{B_n}}{n} + \frac{\delta_{C_n}}{n}\right)} \end{aligned} \quad (50)$$

From Equation (50), we can immediately see that the cosine similarity converges to $\frac{3}{4}$ as n approaches ∞ . For a more rigorous analysis of the convergence rate, we can now consider the variance of the cosine similarity.

For clarity, we can define:

$$\alpha = \frac{\delta_{A_n}}{n}, \beta = \frac{\delta_{B_n}}{n}, \gamma = \frac{\delta_{C_n}}{n} \quad (51)$$

Therefore, Equation (50) becomes:

$$\cos(\theta) \approx \frac{\frac{1}{4} + \alpha}{\frac{1}{3} + \frac{1}{2}(\beta + \gamma)} \quad (52)$$

The denominator of Equation (52), can be further simplified by using Taylor series expansion truncated at the first order terms:

$$\begin{aligned} \frac{1}{3} + \frac{1}{2}(\beta + \gamma) &= \frac{1}{3}(1 + \epsilon), \text{ with } \epsilon = \frac{3}{2}(\beta + \gamma) \\ \Rightarrow \frac{1}{1 + \frac{\epsilon}{3}} &\approx 1 - \epsilon = 1 - \frac{3}{2}(\beta + \gamma) \\ \Rightarrow \frac{1}{\frac{1}{3}(1 + \epsilon)} &\approx 3 - \frac{9}{2}(\beta + \gamma) \quad (53) \end{aligned}$$

We can now substitute Equation (53) in Equation (52) to obtain:

$$\begin{aligned} \cos(\theta) &\approx \left(\frac{1}{4} + \alpha\right) \left(3 - \frac{9}{2}(\beta + \gamma)\right) \approx \\ &\approx \frac{3}{4} + 3\alpha - \frac{9}{8}(\beta + \gamma) \quad (54) \end{aligned}$$

In Equation (54) we neglected the higher order terms of the binomial product as they will diminish faster than first-order terms. Remember that the orders of α, β , and γ are $O\left(\frac{1}{\sqrt{n}}\right)$ (refer to Equation (47)). Therefore, the order of the standard deviation of cosine similarity (Equation (54)) will also be $O\left(\frac{1}{\sqrt{n}}\right)$. This indicates that for $n \rightarrow \infty$, $\cos(\theta)$ converges to $\frac{3}{4} = 0.75$, which is the same results observed in Figure 5 for the real positive case.

The real negative case does not need to be proven as the reasoning will follow the same logic as presented above.

ACKNOWLEDGMENT

The authors would like to thank Prof. Madhusudhan Venkadesan for his valuable feedback during the development of this manuscript.

REFERENCES

- [1] J. X. Chen, 'The Evolution of Computing: AlphaGo', *Comput Sci Eng*, vol. 18, no. 4, pp. 4–7, Jul. 2016, doi: 10.1109/MCSE.2016.74.
- [2] F. Hsu, *Behind Deep Blue: Building the computer that defeated the world chess champion*. Princeton University Press, 2002. Accessed: Apr. 15, 2024. [Online]. Available: https://books.google.com/books?hl=en&lr=&id=zV0W4729UqkC&oi=fnd&pg=PR9&dq=deep+blue+c hess+kasparov&ots=yrHuR4LLI9&sig=GPeoCLW JtJQkfspcvri9q__c5Sc
- [3] D. Silver *et al.*, 'Mastering the game of Go without human knowledge', *Nature* 2017 550:7676, vol. 550, no. 7676, pp. 354–359, Oct. 2017, doi: 10.1038/nature24270.
- [4] J. Vincent, 'DeepMind's AI agents conquer human pros at StarCraft II'. Accessed: Apr. 15, 2024. [Online]. Available: <https://www.theverge.com/2019/1/24/18196135/google-deepmind-ai-starcraft-2-victory>
- [5] J. Jumper *et al.*, 'Highly accurate protein structure prediction with AlphaFold', *Nature* 2021 596:7873, vol. 596, no. 7873, pp. 583–589, Jul. 2021, doi: 10.1038/s41586-021-03819-2.
- [6] J. Kober, J. A. Bagnell, and J. Peters, 'Reinforcement learning in robotics: A survey', *International Journal of Robotics Research*, vol. 32, no. 11, pp. 1238–1274, Sep. 2013, doi: 10.1177/0278364913495721/ASSET/IMAGES/LARGE/10.1177_0278364913495721-FIG8.JPEG.
- [7] A. M. West, F. Tessari, and N. Hogan, 'The Study of Complex Manipulation via Kinematic Hand Synergies: The Effects of Data Pre-Processing', *IEEE Int Conf Rehabil Robot*, vol. 2023, pp. 1–6, Sep. 2023, doi: 10.1109/ICORR58425.2023.10304710.
- [8] J. Bennett and S. Lanning, 'The Netflix Prize', 2007.
- [9] M. Santello, M. Flanders, and J. F. Soechting, 'Postural Hand Synergies for Tool Use', *Journal of Neuroscience*, vol. 18, no. 23, pp. 10105–10115, Dec. 1998, doi: 10.1523/JNEUROSCI.18-23-10105.1998.
- [10] C. R. Mason, J. E. Gomez, and T. J. Ebner, 'Hand Synergies During Reach-to-Grasp', *J Neurophysiol*, 2001, Accessed: Mar. 05, 2023. [Online]. Available: www.jn.org
- [11] J. Ye, 'Cosine similarity measures for intuitionistic fuzzy sets and their applications', *Math Comput Model*, vol. 53, no. 1–2, pp. 91–97, Jan. 2011, doi: 10.1016/J.MCM.2010.07.022.
- [12] A. R. Lahitani, A. E. Permasari, and N. A. Setiawan, 'Cosine similarity to determine similarity measure: Study case in online essay assessment', *Proceedings of 2016 4th International Conference on Cyber and IT Service Management, CITSM 2016*, Sep. 2016, doi: 10.1109/CITSM.2016.7577578.
- [13] P. Xia, L. Zhang, and F. Li, 'Learning similarity with cosine similarity ensemble', *Inf Sci (N Y)*, vol. 307, pp. 39–52, Jun. 2015, doi: 10.1016/J.INS.2015.02.024.
- [14] H. V. Nguyen and L. Bai, 'Cosine Similarity Metric Learning for Face Verification', *Lecture Notes in Computer Science (including subseries Lecture Notes in Artificial Intelligence and Lecture Notes in Bioinformatics)*, vol. 6493 LNCS, no. PART 2, pp. 709–720, 2011, doi: 10.1007/978-3-642-19309-5_55.

- [15] C. Luo, J. Zhan, X. Xue, L. Wang, R. Ren, and Q. Yang, 'Cosine normalization: Using cosine similarity instead of dot product in neural networks', *Lecture Notes in Computer Science (including subseries Lecture Notes in Artificial Intelligence and Lecture Notes in Bioinformatics)*, vol. 11139 LNCS, pp. 382–391, 2018, doi: 10.1007/978-3-030-01418-6_38/FIGURES/6.
- [16] S. Eghbali and L. Tahvildari, 'Fast Cosine Similarity Search in Binary Space with Angular Multi-Index Hashing', *IEEE Trans Knowl Data Eng*, vol. 31, no. 2, pp. 329–342, Feb. 2019, doi: 10.1109/TKDE.2018.2828095.
- [17] Ö. Egecioglu, H. Ferhatosmanoglu, and U. Ogras, 'Dimensionality reduction and similarity computation by inner-product approximations', *IEEE Trans Knowl Data Eng*, vol. 16, no. 6, pp. 714–726, Jun. 2004, doi: 10.1109/TKDE.2004.9.
- [18] Y. S. Lin, J. Y. Jiang, and S. J. Lee, 'A similarity measure for text classification and clustering', *IEEE Trans Knowl Data Eng*, vol. 26, no. 7, pp. 1575–1590, 2014, doi: 10.1109/TKDE.2013.19.
- [19] J. L. W. V. Jensen, 'Sur les fonctions convexes et les inégalités entre les valeurs moyennes', *Acta Mathematica*, vol. 30, no. 1, pp. 175–193, Jan. 1906, doi: 10.1007/BF02418571.
- [20] M. H. De Groot and M. J. Schervish, *Probability and Statistics*, Fourth Edition. Pearson Education, 2014.
- [21] B. Thirey and R. Hickman, 'Distribution of Euclidean Distances Between Randomly Distributed Gaussian Points in n-Space', *ArXiv*, 2015.
- [22] M. Fazle Rabbi, C. Pizzolato, D. G. Lloyd, C. P. Carty, D. Devaprakash, and L. E. Diamond, 'non-negative matrix factorisation is the most appropriate method for extraction of muscle synergies in walking and running', 2020, doi: 10.1038/s41598-020-65257-w.
- [23] M. E. Muller, 'A note on a method for generating points uniformly on n-dimensional spheres', *Commun ACM*, vol. 2, no. 4, pp. 19–20, Apr. 1959, doi: 10.1145/377939.377946.
- [24] G. Marsaglia, 'Choosing a Point from the Surface of a Sphere', <https://doi.org/10.1214/aoms/1177692644>, vol. 43, no. 2, pp. 645–646, Apr. 1972, doi: 10.1214/AOMS/1177692644.



Federico Tessari received a B.Sc. degree (cum laude) in mechanical engineering from Università degli Studi di Roma Tre in 2014, then obtained an M.Sc. degree (cum laude) in mechatronic engineering from Politecnico di Torino in 2016. In 2021, he received his Ph.D. degree (cum laude) in

mechanical engineering from Politecnico di Torino together with the Italian Institute of Technology.

He is currently working as a Senior Post-Doctoral associate at the Massachusetts Institute of Technology. His research interests combine design and control of robotic and wearable devices, with the investigation of the human neuromotor control system.



Kunpeng Yao (Member, IEEE) received the B.Sc. degree from Shanghai Jiao Tong University (SJTU), Shanghai, China, in 2013, the M.Sc. degree from the Technical University of Munich (TUM), Munich, Germany, in 2017, and the Ph.D. degree in Robotics, Control, and Intelligent

Systems from the Swiss Federal Institute of Technology Lausanne (EPFL), Lausanne, Switzerland, in 2022. He is currently a Postdoctoral Fellow at the Newman Laboratory for Biomechanics and Human Rehabilitation, Department of Mechanical Engineering, Massachusetts Institute of Technology (MIT), USA. His primary research interests include robotic dexterous grasping, manipulation, task and motion planning, tactile sensing, and human motor control.

Neville Hogan is Sun Jae Professor of Mechanical Engineering and Professor of Brain and Cognitive Sciences at the Massachusetts Institute of Technology. He earned a Diploma in Engineering (with distinction) from Dublin Institute of Technology and M.S., Mechanical Engineer and Ph.D. degrees from MIT. He joined MIT's faculty in 1979 and presently directs the Newman Laboratory for Biomechanics and Human Rehabilitation. He co-founded Interactive Motion Technologies, now part of Bionik Laboratories.

His research includes robotics, motor neuroscience, and rehabilitation engineering, emphasizing the control of physical contact and dynamic interaction. Awards include: Honorary Doctorates from Delft University of Technology and Dublin Institute of Technology; the Silver Medal of the Royal Academy of Medicine in Ireland; the Saint Patrick's Day Medal for Academia from Science Foundation Ireland; the Henry M. Paynter Outstanding Investigator Award and the Rufus T. Oldenburger Medal from the American Society of Mechanical Engineers, Dynamic Systems and Control Division; and from the Institute of Electrical and Electronics Engineers, the Academic Career Achievement Award from the Engineering in Medicine and Biology Society and the Pioneer in Robotics Award from the Robotics and Automation Society.